Bulletin of the Seismological Society of America, Vol. 100, No. 6, pp. 2978–2995, December 2010, doi: 10.1785/0120090367

A Local Ground-Motion Predictive Model for Turkey, and Its Comparison with Other Regional and Global Ground-Motion Models

by Sinan Akkar and Zehra Çağnan

Abstract We examined the differences between the ground-motion estimations of local and global prediction equations and explored some seismological parameters that may explain these differences. To achieve this objective, we first derived a set of ground-motion prediction equations (GMPEs) for estimating peak horizontal acceleration, velocity, and pseudospectral acceleration using the recently compiled Turkish ground-motion database. The new GMPEs are comparable with the recent global GMPEs in terms of model sophistication, and they are based on a well-studied national dataset. Using global GMPEs from the Next Generation Attenuation of Ground Motions project (Power *et al.*, 2008) and the pan-European Akkar and Bommer (2010) model, we observed that the discrepancy between local and global GMPEs is more prominent at small magnitudes provided that the GMPEs possess similar magnitude limits. Our more detailed comparisons with the pan-European Akkar and Bommer (2010) predictive model, as well as with the estimations from a combined Italian and Turkish accelerometric dataset, indicate that depth can be of importance for delineating the differences between local and global GMPEs.

Introduction

Recent evaluations have shown that empirical ground-motion prediction equations (GMPEs), which are based on well-compiled global strong-motion databanks, estimate comparable ground motions if they are provided a similar level of complexity in their functional forms. For example, Stafford *et al.* (2008) and Campbell and Bozorgnia (2006), who independently explored the level of agreement between the global pan-European and Next Generation Attenuation (NGA) prediction equations, concluded that the NGA equations can be applicable for the seismic hazard estimation of shallow crustal active seismic regions in Europe. Despite the overall agreement between these global models, other evaluations have emphasized that there might be considerable differences between the global European and NGA ground-motion models for some particular earthquake scenarios (Bommer *et al.*, 2010). Similarly, the internal evaluation of NGA models showed significant divergence among each other; as much as a factor of 2 in the case of both large and small magnitude events (Abrahamson *et al.*, 2008). The validity of global GMPEs to different geographical locations also has been questioned by Hintersberger *et al.* (2007) and Drouet *et al.* (2007), thus emphasizing the contrasting arguments because the latter study confirmed the application of such GMPEs to geographical regions outside their zone of origin while the former study showed cases opposite to this finding. These studies highlight the continuing need of GMPEs to include more sophisticated parameters in terms of distance, style of faulting, site classification, etcetera, to delineate regional differences more objectively (Douglas, 2007). Perhaps a more important conclusion of these studies is the significance of epistemic uncertainty requiring the consideration of a set of predictive equations for a better quantification of seismic hazard in a region. As indicated in Bommer *et al.* (2010), this fact can be more crucial, in particular for regions of low seismicity with relatively scarce data.

One way of accounting for epistemic uncertainty while determining the regional seismic hazard levels can be the utilization of both region-specific and global GMPEs. This task would require more elaborate regional predictive equations that are compatible with the general features of global GMPEs. A good example for such an effort is the recent prediction equation of Bindi *et al.* (2010). This GMPE is derived from one of the latest versions of the Italian strong-motion database (Luzi *et al.*, 2008), and it is tailored with the new developments in ground-motion modeling. Similar efforts for the enhancement of strong-motion databases are being carried out both in other national projects (e.g., Akkar *et al.*, 2010) and international projects (the Seismic Harmonization in Europe—European Community 7th Framework Program

Project and the Network of Research Infrastructures for European Seismology—European Community 6th Framework Program Project). Inherently, the main target of national projects is to produce improved GMPEs that can be integrated with the global predictive models. A typical illustration about the necessity of improving local GMPEs is presented in Figure 1. This figure shows the residual scatters of previously computed Turkish GMPEs to verify their performance by using the recently compiled Turkish strong-motion database (Akkar *et al.*, 2010; see also the Data and Resources section). Major features of these GMPEs are given in Table 1, and the residual analyses were done by considering their limitations described by the model developers. The GMPEs were derived from the older versions of Turkish accelerometric data and tend to overestimate the ground motions that can be attributed to the assumptions made by their developers due to insufficient level of database knowledge (i.e., estimated site conditions, source-to-site distance metrics, and hybrid magnitude scaling; Akkar *et al.*, 2010) at the time they were derived.

In this article, we first derived a set of predictive equations from the aforementioned new Turkish strong-motion database. The equations are valid for a distance (Joyner–Boore distance, R_{jb}) range of 0–200 km and are derived for moment magnitudes between $5 \leq \mathbf{M} \leq 7.6$. They consider the effects of nonlinear soil behavior and style of faulting and can be considered as a good example for local GMPEs that are derived from a well-studied regional database. We then compared the new GMPEs with the global NGA and pan-European (i.e., Akkar and Bommer, 2010) GMPEs to address the differences between regional and global ground-motion models in terms of some important seismological

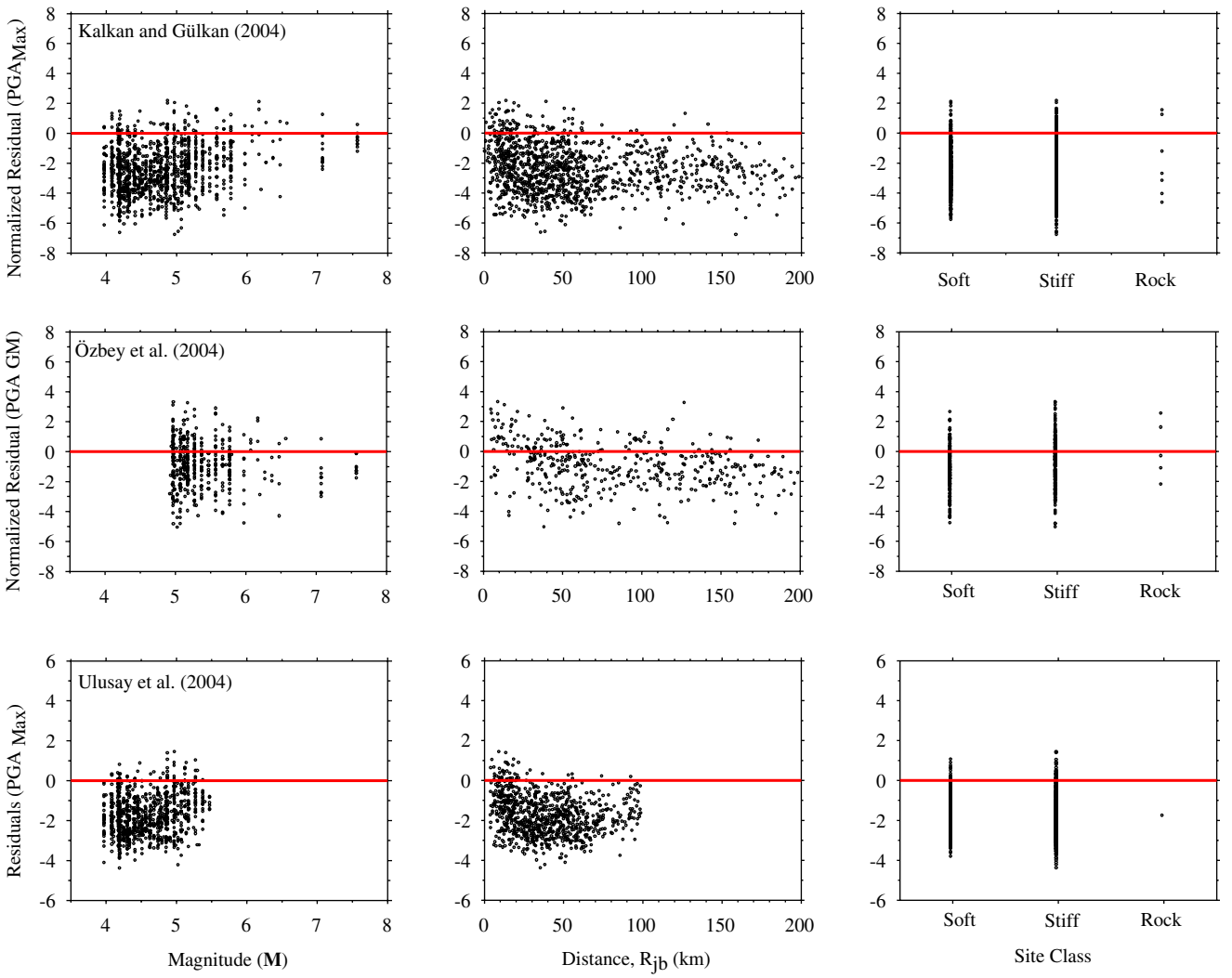

Figure 1. Normalized residual scatters of GMPEs that are proposed by Kalkan and Gülkan (2004), Özbey *et al.* (2004), and Ulusay *et al.*, (2004). The residuals of Ulusay *et al.*, (2004) could not be presented in the normalized form because this study does not report the standard deviation. The residual scatters show significant bias toward conservative estimations for magnitude, distance, and site class estimator parameters. (Note: our comparisons include aftershock records, and originally aftershock events were not considered in Kalkan and Gülkan, 2004). The color version of this figure is available only in the electronic edition.

Table 1
List of Compared GMPEs with Important Features

Study	Abbreviation*	Region†	N_R, N_E‡	Component§	M, M_{min}, M_{max}‖	R, R_{min}, R_{max}#	Fault**	Site††
Abrahamson and Silva (2008)	AS08	Worldwide (MS and AS)	2754, 135	PGA, PGV, PSA in GMRotI50	**M**, 5.0, 8.5	R_{rup}, 0, 200	SS, N, R	V_{S30}: 180 m/s to 2000 m/s
Akkar and Bommer (2010)	AB10	Euro-Med (MS and AS)	532, 131	PGA_{GM}, PGV_{GM}, PSA_{GM}	**M**, 5.0, 7.6	R_{jb}, 0, 100	SS, N, R	R, ST, SF
Bindi *et al.* (2010)	Betal10	Italy (MS and AS)	561, 107	PGA_{Max}, PGV_{Max}, PSA_{Max}, PGA_{Ver}, PGV_{Ver}, PSA_{Ver},	**M**, 4.0, 6.9	R_{jb}, 0, 100	SS, N, R	R, SA, DA
Boore and Atkinson (2008)	BA08	Worldwide (MS)	1574, 58	PGA, PGV, PSA in GMRotI50	**M**, 5.0, 8.0	R_{jb}, 0, 200	SS, N, R	V_{S30}: 180 m/s to 1300 m/s
Campbell and Bozorgnia (2008)	CB08	Worldwide (MS and AS)	1561, 64	PGA, PGV, PSA in GMRotI50	**M**, 4.0, 8.5	R_{rup}, 0, 200	SS, N, R	V_{S30}: 180 m/s to 1500 m/s
Chiou and Youngs (2008)	CY08	Worldwide (MS and AS)	1950, 125	PGA, PGV, PSA in GMRotI50	**M**, 4.0, 8.5	R_{rup}, 0, 200	SS, N, R	V_{S30}: 150 m/s to 1500 m/s
Idriss (2008)	I08	Worldwide (MS and AS)	942, 72	PGA, PSA in GMRotI50	**M**, 4.5, 8.0	R_{rup}, 0, 200	SS, R	V_{S30}: 450 m/s to 900 m/s
Kalkan and Gülkan (2004)	KG04	Turkey (MS)	112, 57	PGA_{Max}, PSA_{Max}	**M**, 4.0, 7.4	R_{jb}, 1.2, 250	U	R, ST, SF
Özbey *et al.* (2004)	Oetal04	NW Turkey (MS and AS)	195, 17	PGA_{GM}, PSA_{GM}	**M**, 5.0, 7.4	R_{jb}, 5, 300	U	R, ST, SF
Ulusay *et al.* (2004)	Uetal04	Turkey (MS and AS)	211, 122	PGA_{Max}	**M**, 4.1, 7.5	R_{epi}, 5, 100	U	R, ST, SF

*Abbreviations of GMPEs used in this study.

†MS and AS indicate the inclusion of mainshock and aftershock data in the development of GMPEs.

‡N_R, number of records; N_E, number of earthquakes in the dataset.

§GMRotI50, rotation-independent average horizontal component (Boore *et al.*, 2006); subscripts Max and GM, maximum and geometric mean of horizontal components, respectively; subscript Ver refers to vertical component.

‖M, magnitude scaling; M_{min} and M_{max}, minimum and maximum magnitude range of GMPEs; **M**, moment magnitude.

#R, distance metric; R_{min} and R_{max}, minimum and maximum distance range of GMPEs; R_{rup}, closest distance to rupture surface; R_{jb}, closest distance to horizontal projection of rupture surface; R_{epi}, epicentral distance.

**SS, strike-slip; N, normal faulting; R, reverse faulting; T, thrust faulting; U, faulting style is either unknown or not considered in GMPE.

††V_{S30}, average shear-wave velocity in the upper 30 m soil profile; R, rock; SA, shallow alluvium; DA, deep alluvium; ST, stiff soil; SF, soft soil.

parameters. To describe the possible regional differences in our model with respect to the global GMPEs considered, we particularly focused on the pan-European ground-motion model and compared its estimations in more detail with those of this study, as well as to the ground motions estimated from the combined dataset of Turkish and Italian strong-motion recordings (see Data and Resources section). Our statistical observations on the fundamental seismological parameters of these strong-motion databases suggest that depth can be of importance to highlight the regional differences even for crustal events. We would like to stress that the aim of discussions presented here is not to promote the use of poorly-constrained local models in order to account for the regional effects on ground-motion estimations. On the contrary, we emphasize the usefulness of reliable local models that are based on well-studied large datasets and encourage their use with global GMPEs to reduce the modeling uncertainty while estimating the hazard for the particular region of interest.

Strong-Motion Databank

The databank used in this study is compiled within the framework of the project entitled "Compilation of Turkish Strong-Motion Network According to the International Standards" (see Data and Resources section). The procedures followed to assemble the database are described in Akkar *et al.* (2010) and Sandıkkaya *et al.* (2010). The database contains 1259 records from 573 earthquakes with moment magnitude and source-to-site distance ranges of $3.5 \le \mathbf{M} \le 7.6$ and $0 \text{ km} \le R_{jb} \le 200$ km (Fig. 2a,b). A significant portion of the data pertains to recordings of small events with $\mathbf{M} < 5$. The two largest magnitude events in the database are the 1999 Düzce ($\mathbf{M}$ 7.1) and Kocaeli ($\mathbf{M}$ 7.6) earthquakes whose ground motions exhibit relatively low-amplitude peak motions when compared with other similar size earthquakes, elsewhere. The low-amplitude waveforms were attributed to the observed surface rupture in these events (Kagawa *et al.*, 2004). The majority of the ground motions are from National Earthquake Hazards Reduction Program (Building Seismic Safety Council, 2009) site classifications C ($360 \text{ m/s} \le V_{S30} < 760$ m/s) and D ($180 \text{ m/s} \le V_{S30} < 360$ m/s). There are very few waveforms with $V_{S30} \ge 760$ m/s. As illustrated in Figure 2b, the database is dominated by the strike-slip events (70% of the entire dataset). Records corresponding to normal events make up 28% of the database, and records corresponding to reverse/thrust events constitute only 2% of the database. Another distinct feature of our database is the higher percentage of singly recorded events that, for example, exceeds the corresponding percentage in the pan-European strong-motion database of Akkar and Bommer (2010) by a factor of 2. The reader is referred to Akkar *et al.* (2010) and Sandıkkaya *et al.* (2010) for a detailed view about the Turkish strong-motion database.

Functional Form

We explored several functional forms, trying to keep a balance between a rigorous model (for meaningful and reliable estimations) and a robust expression (for wider implementation in engineering applications). Equation (1) shows our basic expression for the geometric mean estimations of peak horizontal ground acceleration (PGA_{GM}), velocity (PGV_{GM}) and pseudoacceleration spectral ordinates (PSA_{GM}). This functional form is the base model in Abrahamson and Silva (1997, 2008) and contains terms that account for saturation and magnitude-dependent decay effects.For $\mathbf{M} \le c_1$:

$$\ln(Y) = a_1 + a_2(\mathbf{M} - c_1) + a_4(8.5 - \mathbf{M})^2 + [a_5 + a_6(\mathbf{M} - c_1)] \ln \sqrt{R_{jb}^2 + a_7^2} + a_8 F_N + a_9 F_R. \quad (1a)$$

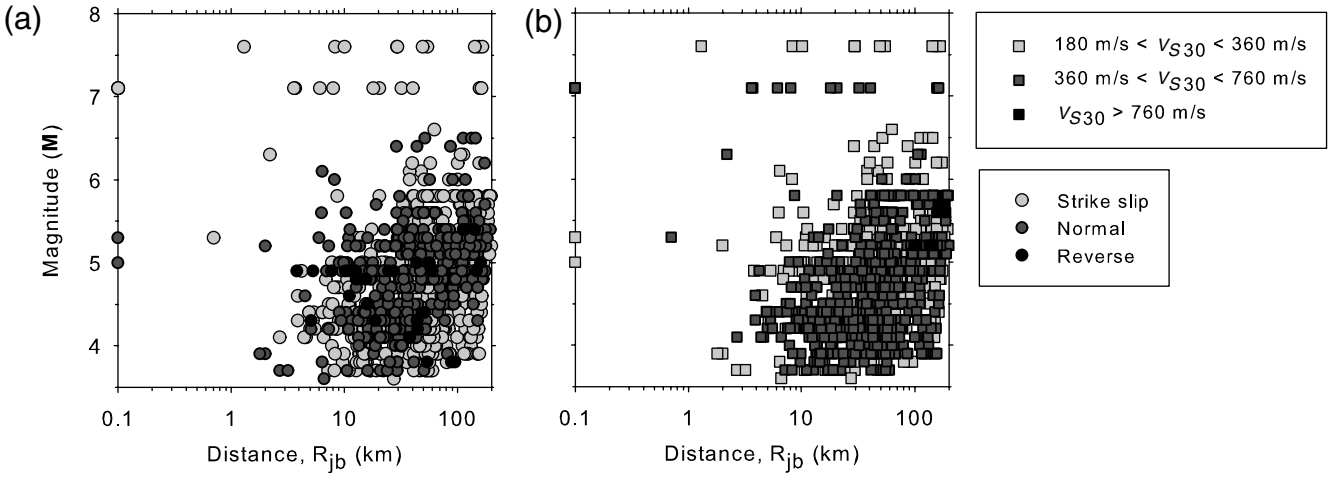

Figure 2. Magnitude versus distance scatters (a) for site class and (b) for faulting style of the Turkish strong-motion database.

For $\mathbf{M} > c_1$:

$$\ln(Y) = a_1 + a_3(\mathbf{M} - c_1) + a_4(8.5 - \mathbf{M})^2 + [a_5 + a_6(\mathbf{M} - c_1)] \ln \sqrt{R_{\text{jb}}^2 + a_7^2} + a_8 F_N + a_9 F_R. \quad (1b)$$

In equation (1), the multiplier of the logarithmic distance term accounts for the magnitude-dependent ground-motion decay. It also controls the saturation of high-frequency ground motions at short distances (Abrahamson and Silva, 1997). The long-period component behavior of ground motions are controlled by the linear and quadratic magnitude terms in the functional form. The constant c_1 is the reference magnitude, and it is fixed to 6.5 in this study. The parameters F_N and F_R are dummy variables for the influence of faulting, taking values of 1 for normal and reverse faults and zero otherwise.

Given the fully defined V_{S30} values at each station, we described the linear and nonlinear site effects by the site response function used in Boore and Atkinson (2008) (hereafter referred to as BA08). The original form of this model is proposed by Choi and Stewart (2005). We choose this site response model among various alternatives due to its simplicity and its fairly good performance with our strong-motion database. This is illustrated by the distribution of normalized intraevent residuals of BA08 that are computed for the PGA and PGV values in our database (Fig. 3). The intraevent residuals consistently yield conservative values (see the histogram plots and residual distributions presented in Fig. 3), but they do not exhibit any significant bias with the changes in V_{S30}. This is also illustrated by the good match between the histograms and the superimposed normal probability plots fitted to the normalized residuals. Exceptions to this observation are the few sites with $V_{S30} > 720$ m/s. Strictly speaking, it would be difficult to assess the performance of chosen site response model for high V_{S30} values because the database contains only few sites with $V_{S30} > 720$ m/s. The consistent overestimation by the BA08 model, in fact, points a general feature of our database: as stated previously, the ground motions in our database define an amplitude pattern relatively lower than other similar size events occurred around the world. This will be discussed in detail in the following sections of the paper.

The general form of the site response function (F_S) is given in equations (2), (3), and (4) for completeness:

$$F_S = F_{\text{LIN}} + F_{\text{NL}} \quad (2)$$

$$F_{\text{LIN}} = b_{\text{lin}} \ln\left(\frac{V_{S30}}{V_{\text{ref}}}\right) \quad (3)$$

$$F_{\text{NL}} = b_{\text{nl}} \ln\left(\frac{\text{pga}_{\text{low}}}{0.1}\right), \qquad \text{pga4nl} \le 0.03g \quad (4a)$$

$$F_{\text{NL}} = b_{\text{nl}} \ln\left(\frac{\text{pga}_{\text{low}}}{0.1}\right) + c\left[\ln\left(\frac{\text{pga4nl}}{0.03}\right)\right]^2 + d\left[\ln\left(\frac{\text{pga4nl}}{0.03}\right)\right]^3, \; 0.03g < \text{pga4nl} \le 0.09g \quad (4b)$$

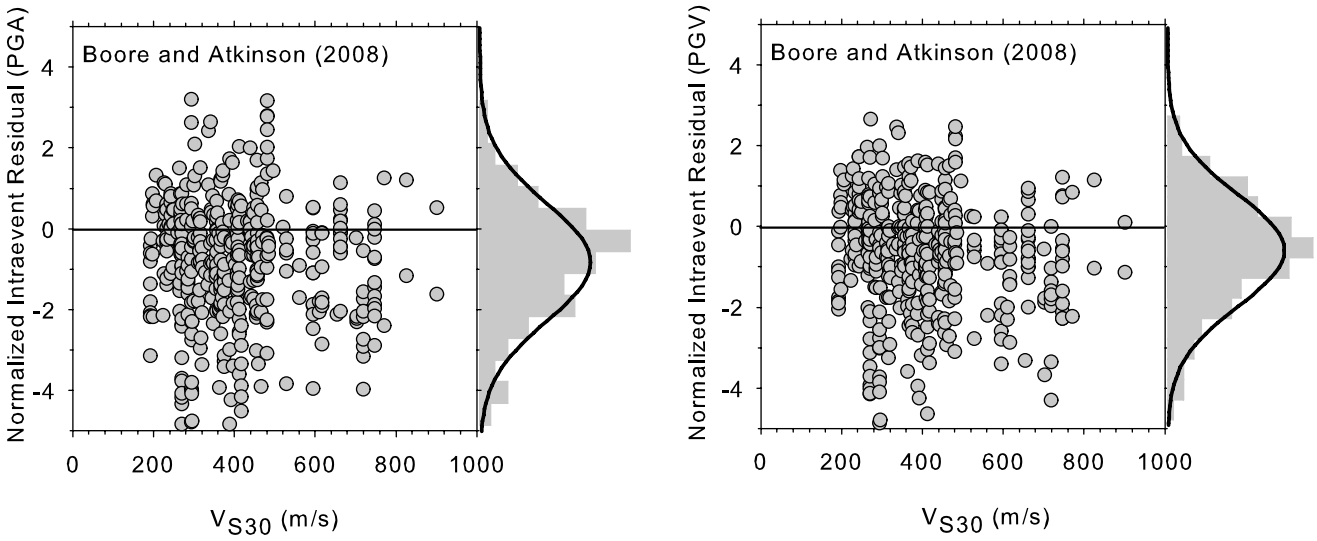

Figure 3. Variation of intraevent PGA_{GM} and PGV_{GM} residuals [ln(observed/estimated)] as a function of V_{S30} that are computed from the BA08 estimations. Different component definitions of our database and that of BA08 (GMRotI50, the rotation-independent average horizontal component of Boore *et al.*, 2006) do not require adjustments in residual calculations because the median values of BA08 have been demonstrated to be equivalent to those from the geometric mean definition used in our study (Beyer and Bommer, 2006). (See Table 1 for additional abbreviations.)

$$F_{NL} = b_{nl} \ln\left(\frac{\text{pga4nl}}{0.1}\right), \qquad \text{pga4nl} > 0.09g. \qquad (4c)$$

The site amplification function consists of a linear (F_{LIN}) and a nonlinear (F_{NL}) term; pga4nl is the predicted PGA in g for $V_{S30} = 760$ m/s (V_{ref}); b_{lin}, b_1, and b_2 are coefficients that are given in Table 2; $\text{pga}_{low}(= 0.06g)$ is an intermediate acceleration value that accounts for the transition between linear and nonlinear soil behavior; b_{nl} depends on both peak ground motion and V_{S30} values. The explicit forms of coefficients c, d, and b_{nl} are not given here for space considerations (see Boore and Atkinson, 2008 for details).

Modeling Details: Sigma, **M** Threshold, Period Range and Style of Faulting

After the emphasis of magnitude effect on the aleatory variability (Youngs *et al.*, 1995), many model developers have derived their GMPEs with magnitude-dependent sigma (e.g., Abrahamson and Silva, 1997; Campbell, 1997; Ambraseys *et al.*, 2005; Akkar and Bommer, 2007a, 2007b; Abrahamson and Silva, 2008). The reader is referred to Strasser *et al.* (2009) for a detailed review of studies on the description of aleatory variability in ground-motion models. In this study, we explored the magnitude dependence of sigma in our dataset using pure error analysis that was initially adopted by Douglas and Smit (2001) for ground-motion variability. We partitioned the magnitude–distance space into different bin sizes to observe the sensitivity of magnitude-dependent sigma to the binning scheme. This way, we assessed whether the magnitude dependency is a specific feature of our database; an approach that has already been applied by Bommer *et al.* (2007). Our findings from this exercise are similar to those of the aforementioned study, indicating a significant variation in magnitude-dependent sigma based on the adopted binning scheme. (For some specific cases, we even observed an increase in sigma with increasing magnitude, a trend that is contrary to the well-recognized variation of magnitude-dependent aleatory variability.) These observations led us to disregard magnitude dependency in sigma.

Table 2
Soil Amplification Model Coefficients Suggested by Boore and Atkinson (2008)

Period (s)	b_{lin}	b_1	b_2
PGA_{GM}	−0.36	−0.64	−0.14
PGV_{GM}	−0.60	−0.50	−0.06
0.03	−0.33	−0.62	−0.11
0.05	−0.29	−0.64	−0.11
0.075	−0.23	−0.64	−0.11
0.10	−0.25	−0.60	−0.13
0.15	−0.28	−0.53	−0.18
0.20	−0.31	−0.52	−0.19
0.25	−0.39	−0.52	−0.16
0.30	−0.44	−0.52	−0.14
0.40	−0.50	−0.51	−0.10
0.50	−0.60	−0.50	−0.06
0.75	−0.69	−0.47	0.00
1.00	−0.70	−0.44	0.00
1.50	−0.72	−0.40	0.00
2.00	−0.73	−0.38	0.00

Recent studies have shown that large-magnitude databases tend to overestimate the ground motions of low-seismicity, depending on the center of the dataset (Bommer *et al.*, 2007; Atkinson and Morrison, 2009). Rapid decay of small magnitude events with distance and different ground-motion amplitude scaling between small and large magnitudes are defined as the two major factors for the discrepancies between GMPEs derived from small-magnitude and large-magnitude recordings (Cotton *et al.*, 2008). Based on these findings, we primarily intended to derive a model to capture the influence of small-magnitude and large-magnitude events on hazard estimation in an unbiased manner. We first derived PGA_{GM} and PGV_{GM} GMPEs using magnitude thresholds of **M** 3.5, **M** 4.0, **M** 4.5, and **M** 5.0. We focused on PGA and PGV in our sensitivity analyses as they can represent high-to-intermediate frequency ground-motion components, yielding a fairly rapid view about the influence of magnitude threshold on our model. The sensitivity analyses showed that GMPEs derived from the largest magnitude threshold (i.e., the dataset with $5.0 \le \mathbf{M} \le 7.6$) tend to overestimate the ground motions derived from the lower magnitude thresholds. Although this is consistent with the previous findings as indicated previously in this article, the ground-motion amplitudes estimated from lower magnitude thresholds follow a complicated order for **M** 4 comparisons (Fig. 4). The PGA_{GM} and PGV_{GM} estimates from the $4.5 \le \mathbf{M} \le 7.6$ dataset are lower with respect to ground motions estimated from the datasets assembled using the recordings of $3.5 \le \mathbf{M} \le 7.6$ and $4.0 \le \mathbf{M} \le 7.6$. This is contrary to the expected trends observed in the relevant studies (e.g., Bommer *et al.*, 2007; Atkinson and Morrison, 2009). Besides, our observations did not show any indication about the reduction of discrepancy between small-magnitude and large-magnitude threshold GMPEs with the increase in magnitude level. Speculatively, these observations could be attributed to the magnitude scaling specific to the crustal variations in Turkey. However, the bulk of the databank that results in a non-uniform magnitude distribution (Fig. 2a,b) led us to consider the larger magnitude data with $\mathbf{M} \ge 5$ for the derivation of our GMPEs. Accordingly, a total of 433 accelerograms from 137 events (consisting of 102 mainshocks with 346 recordings and 35 aftershocks with 88 recordings) were considered in our regression analysis. We used the maximum likelihood methodology (Joyner and Boore, 1993) for the calculation of regression coefficients. Table 3 lists the regression coefficients and the standard deviations of the GMPEs derived for PGA_{GM}, PSA_{GM}, and PGV_{GM}.

We derived spectral ordinate prediction equations for $0.03 \text{ s} \le T \le 2.0$ s. The data become scarce for $T > 2.0$ s when the Akkar and Bommer (2006) criteria are used for minimizing the low-cut (high-pass) filtering effects on elastic

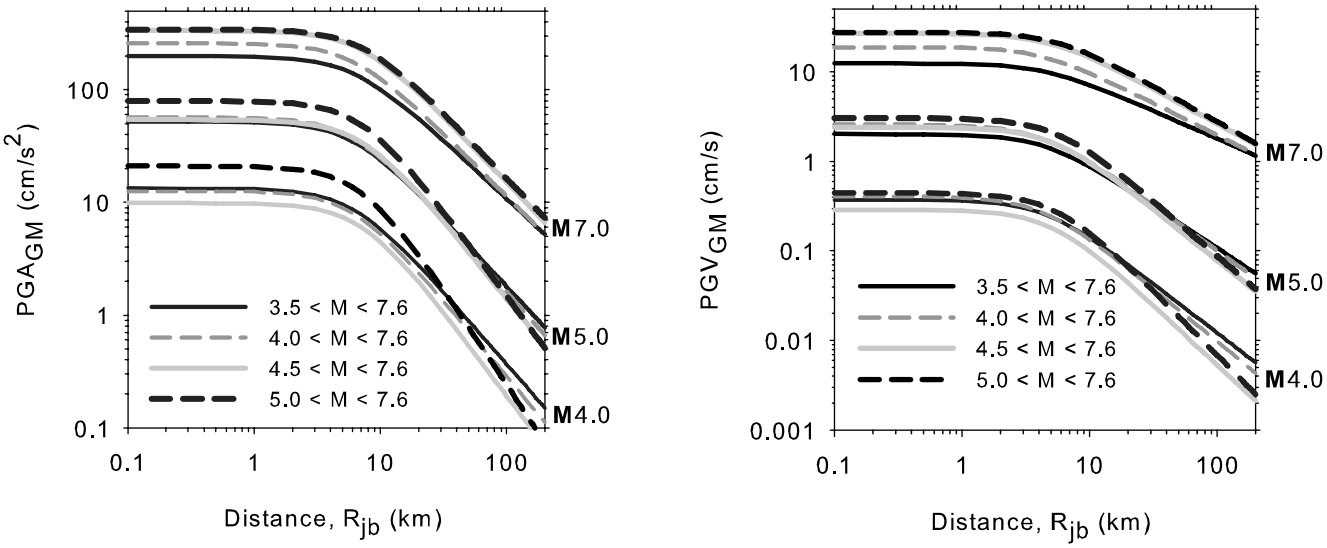

Figure 4. Comparisons of PGA_{GM} (left panel) and PGV_{GM} (right panel) estimations from our strong-motion dataset using different magnitude thresholds (distance range is the same in all models; $R_{jb} \leq 200$ km). The comparisons are for a rock site ($V_{S30} = 760$ m/s) and strike-slip faulting style.

spectral ordinates. The decision on the limiting short period (i.e., $T = 0.03$ s) is based on the Nyquist and high-cut (low-pass) filtering frequencies of the accelerograms. Except for some old analog recordings, the sampling frequencies of almost all accelerograms are either equal to or greater than 100 Hz, and high-cut filter values are generally above 30 Hz (Erdoğan, 2008). We note that our choice of $T = 0.03$ s, as the shortest period value, can be considered as conservative based on a recent study by Douglas and Boore (2010). The PGA values can also be affected by high-cut filtering. Our PGA comparisons before and after the application of high-cut filtering showed negligible differences, suggesting the reliability of PGA values employed in the regression analysis.

The style-of-faulting coefficients (a_8 and a_9 for normal and reverse faulting, respectively) presented in Table 3 indicate smaller horizontal ground-motion amplitudes for normal (N) events when compared to strike-slip (SS) and reverse (R) faulting cases. Figure 5 compares our N:SS and R:SS ratios with those obtained from the NGA and pan-European global models for small (**M** 5) and large (**M** 7) magnitude events (see fundamental features of these models in Table 1). Although our model does not account for hanging-wall effects, we considered it in our comparisons for the NGA models because many NGA equations incorporate this kinematic property for dipping faults. (The reader is referred to the figure caption for details of the scenario events.) Except for a few cases, the comparisons depict a fairly good match between our findings and those reported by the other models. Nevertheless, given the relatively small number of reverse faulting records in the dataset, the style-of-faulting dependency of our GMPEs can be subject to further refinements with the accumulation of reverse fault events in the dataset.

Figure 6 shows the period-dependent comparisons of our sigma with the models discussed in Figure 5. We additionally included the standard deviations of Bindi *et al.* (2010), another regional model, in these comparisons. Comparisons are done for small (**M** 5) and large (**M** 7) magnitude scenarios whose detailed descriptions are given in the figure caption. In general, our sigma values and those of Bindi *et al.* (2010) are larger with respect to the other models of comparison. This is better observed at the higher magnitudes because neither Bindi *et al.* (2010) nor our model tend to reduce the aleatory variability for larger magnitudes, as in the case of NGA models. Larger sigma in local models can be attributed to the dataset features or the selected explanatory variables in the functional form. However, when the overall sigma variation is of concern, our sigma values are within the expected limitations among those reported in other GMPEs that have been published over the last four decades (Strasser *et al.*, 2009).

Evaluation of Proposed GMPEs

We verified our prediction equations by residual analysis. Figure 7 shows the interevent and intraevent residuals of PGA_{GM}, PGV_{GM}, and PSA_{GM} at $T = 0.2$ s and $T = 1.0$ s. Here, the PGA_{GM} and PSA_{GM} at $T = 0.2$ s residuals represent the performance of our high-frequency ground-motion estimations. Similarly, the PGV_{GM} and PSA_{GM} at $T = 1.0$ s residuals are used to assess the performance of intermediate-frequency to low-frequency ground-motion estimations. The residual plots show straight lines fitted to the residuals (dashed lines) as well as the variations of average residuals for constant intervals of estimator parameters in log-space (solid lines). These lines facilitate the observations on the tendency of residuals with the changes in independent

Table 3
Regression Coefficients of Equation (1) for the GMPEs Derived in This Study

$T(S)$	a_1	a_2	a_3	a_4	a_5	a_6	a_7	a_8	a_9	σ^*	τ^*	$\sigma_{Tot}{}^\dagger$
PGA_{GM}	8.92418	−0.513	−0.695	−0.18555	−1.25594	0.18105	7.33617	−0.02125	0.01851	0.6527	0.5163	0.8322
0.03	8.85984	−0.513	−0.695	−0.17123	−1.25132	0.18421	7.46968	−0.0134	0.03512	0.6484	0.5148	0.8279
0.05	9.05262	−0.513	−0.695	−0.15516	−1.28796	0.1984	7.26552	0.02076	0.01484	0.6622	0.5049	0.8327
0.075	9.56670	−0.513	−0.695	−0.13840	−1.38817	0.20246	8.03646	0.07311	0.02492	0.6849	0.5144	0.8566
0.10	9.85606	−0.513	−0.695	−0.11563	−1.43846	0.21833	8.84202	0.11044	−0.00620	0.7001	0.5182	0.871
0.15	10.43715	−0.513	−0.695	−0.17897	−1.46786	0.15588	9.39515	0.03555	0.19751	0.6958	0.549	0.8863
0.20	10.63516	−0.513	−0.695	−0.21034	−1.44625	0.11590	9.60868	−0.03536	0.18594	0.6963	0.5562	0.8912
0.25	10.12551	−0.513	−0.695	−0.25565	−1.27388	0.09426	7.54353	−0.10685	0.13574	0.7060	0.5585	0.9002
0.30	10.12745	−0.513	−0.695	−0.27020	−1.26899	0.08352	8.03144	−0.10685	0.13574	0.6718	0.5735	0.8833
0.40	9.47855	−0.513	−0.695	−0.30498	−1.09793	0.06082	6.24042	−0.11197	0.16555	0.6699	0.5857	0.8898
0.50	8.95147	−0.513	−0.695	−0.29877	−1.01703	0.09099	5.67936	−0.10118	0.23546	0.6455	0.5782	0.8666
0.75	8.10498	−0.513	−0.695	−0.3349	−0.84365	0.08647	4.93842	−0.0456	0.10993	0.6463	0.6168	0.8934
1.00	7.61737	−0.513	−0.695	−0.35366	−0.75840	0.09623	4.12590	−0.01936	0.19729	0.6485	0.6407	0.9116
1.50	7.20427	−0.513	−0.695	−0.39858	−0.70134	0.11219	3.46535	−0.02618	0.21977	0.6300	0.6751	0.9234
2.00	6.70845	−0.513	−0.695	−0.39528	−0.70766	0.12032	3.8822	−0.03215	0.20584	0.6243	0.6574	0.9066
PGV_{GM}	5.60931	−0.513	−0.695	−0.25800	−0.90393	0.21576	5.57472	−0.10481	0.07791	0.6154	0.526	0.8096

*σ and τ are intraevent and interevent standard deviations, respectively.
†The total sigma (σ_{Tot}) is calculated as $\sigma_{Tot} = \sqrt{\sigma^2 + \tau^2}$.

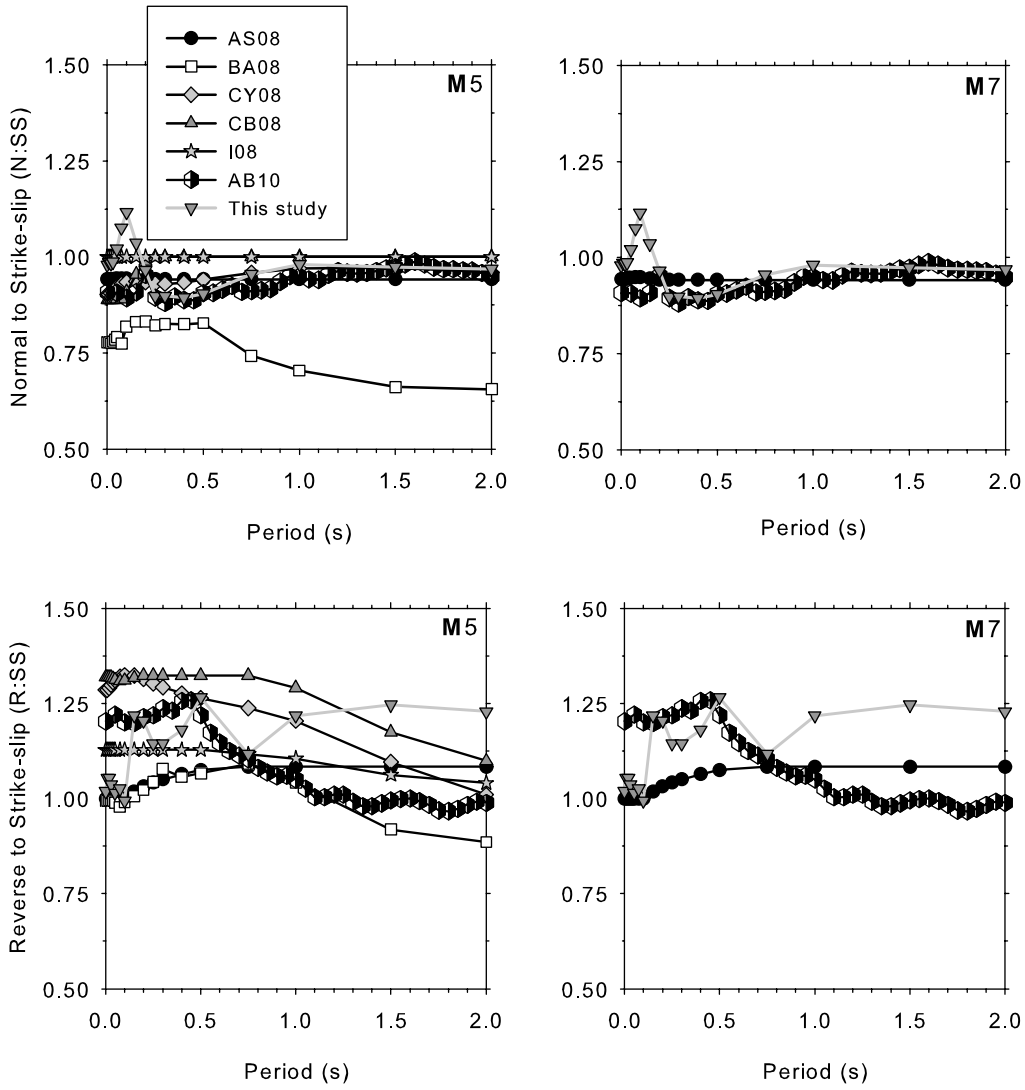

Figure 5. Comparisons of normal to strike-slip (top row) and reverse to strike-slip ground-motion estimations for scenario earthquakes of **M** 5 (left column) and **M** 7 (right column) at a rock site (V_{S30} = 760 m/s) located 10 km (R_{rup}) from the source (corresponding R_{jb} is calculated from the given fault geometry). The faults dip with an angle of 45°. For NGA models of AS08, CB08, and CY08 that consider the magnitude-dependent depth to top-of-rupture (Z_{TOR}) effect, we used the median Z_{TOR} values recommended by Abrahamson *et al.* (2008). We also considered the hanging-wall influence that is explicitly accounted for by AS08, CB08, and CY08.

regression parameters. We show the p values in each plot to reject or fail-to-reject the null hypothesis of unbiased estimations. The results are discussed for a level of significance of 0.05. Interevent residuals that describe the earthquake-to-earthquake variability do not exhibit significant bias with the changes in magnitude (top panels in Fig. 7). The increase in vibration period (i.e., T = 1.0 s) results in unsafe estimations for increasing magnitude. However, the calculated p value still favors the fail-to-reject decision for the null hypothesis. Similarly, the intraevent residuals (record-specific variability) against distance (middle panels in Fig. 7) suggest unbiased estimations of our GMPEs for the entire frequency band of interest. The intraevent residuals against the V_{S30} variations (bottom row in Fig. 7), on the other hand, suggest that the increase in vibration periods (T = 1.0 s in this case) result in conservative estimations; in particular for V_{S30} > 450 m/s. The increase in V_{S30} associated with longer periods invokes the linear site amplification term in the chosen site response function. We note that the linear site term in our model is V_{S30}-dependent (equation 3), and the regional differences in V_{S30}, as a proxy to define site effects, can be speculated to be a reason for the observed bias toward stiffer sites and longer vibration periods. As a matter of fact, the interstation residuals (Fig. 8) of the outlier stations[1] detected among the strong-motion sites used in our GMPEs tend toward the more conservative side with increasing

[1]We ran interstation residual analysis for the entire period band of interest. These analyses indicated that for high frequencies ($T \leq 0.5$ s) the interstation residuals generally were distributed in the range ±0.6 and for low frequencies in the range ±2.0. We described the stations with residuals mostly varying outside these ranges as outlier stations.

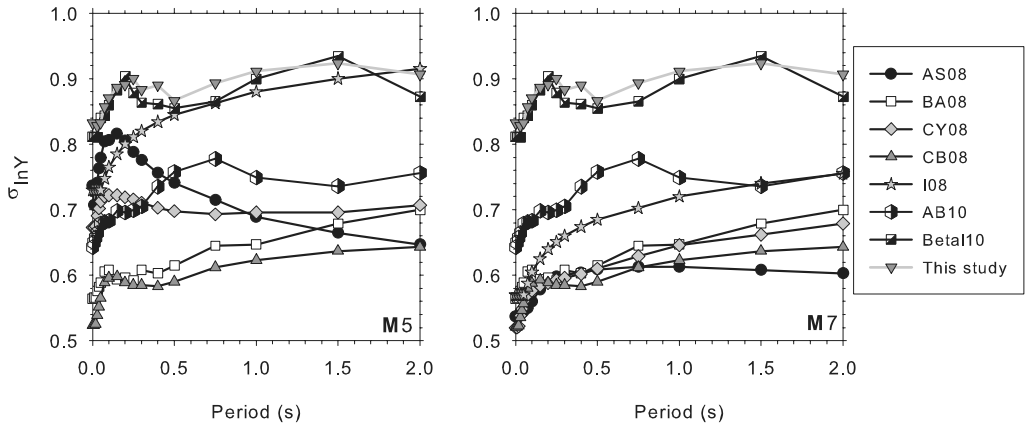

Figure 6. Comparative small-magnitude (**M** 5, on the left) and large-magnitude (**M** 7, on the right) sigma variations between this study and the global NGA and pan-European predictive models, as well as the recent Italian model (Bindi *et al.*, 2010). Comparisons are for a rock site (V_{S30} = 760 m/s) of strike-slip earthquakes (with a dip of 90°) at a distance of R_{rup} = 10 km. We used the median depth to top-of-rupture values recommended in Abrahamson *et al.* (2008) for AS08, CB08, and CY08.

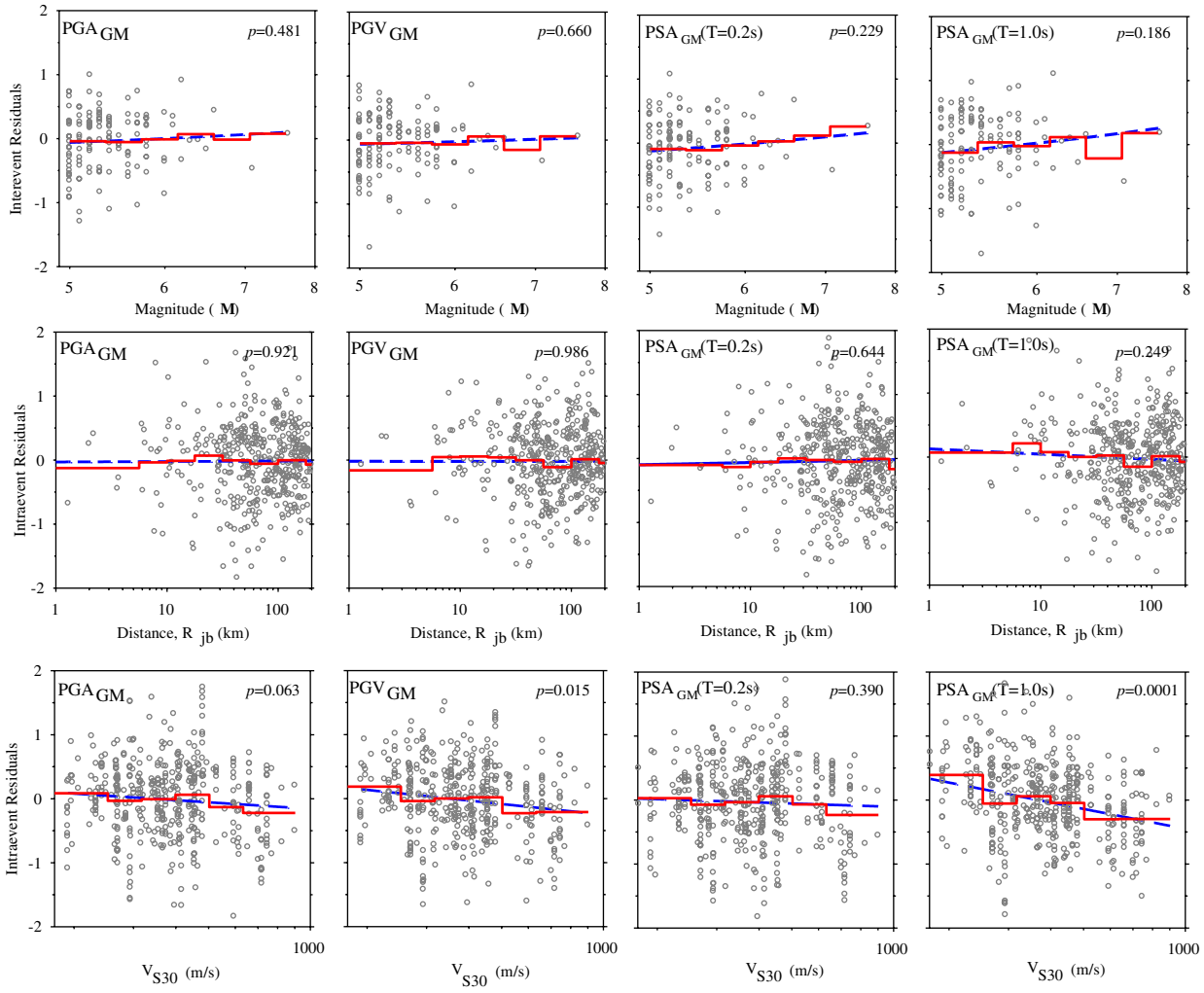

Figure 7. Interevent (top row) and intraevent (last two rows) residuals for PGA_{GM} (first column), PGV_{GM} (second column), PSA_{GM} (T = 0.2 s) (third column), and PSA_{GM}(T = 1.0 s) (fourth column). Dashed straight lines are the least square fits. The solid lines show the average variation of residuals for equally spaced log intervals. The p values for testing the null hypothesis about the likely existence/nonexistence of bias in estimations are shown on the upper right corner of each plot. The color version of this figure is available only in the electronic edition.

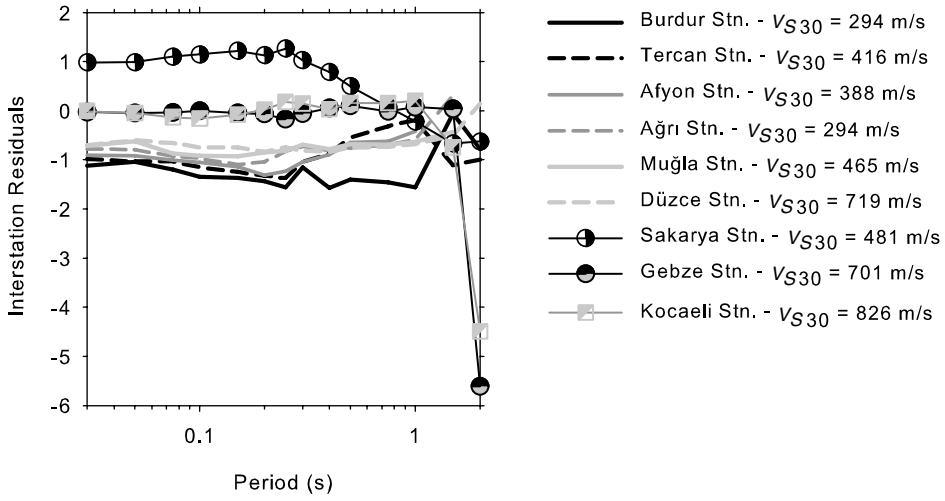

Figure 8. Period-dependent interstation residuals of the outlier stations detected in our GMPEs.

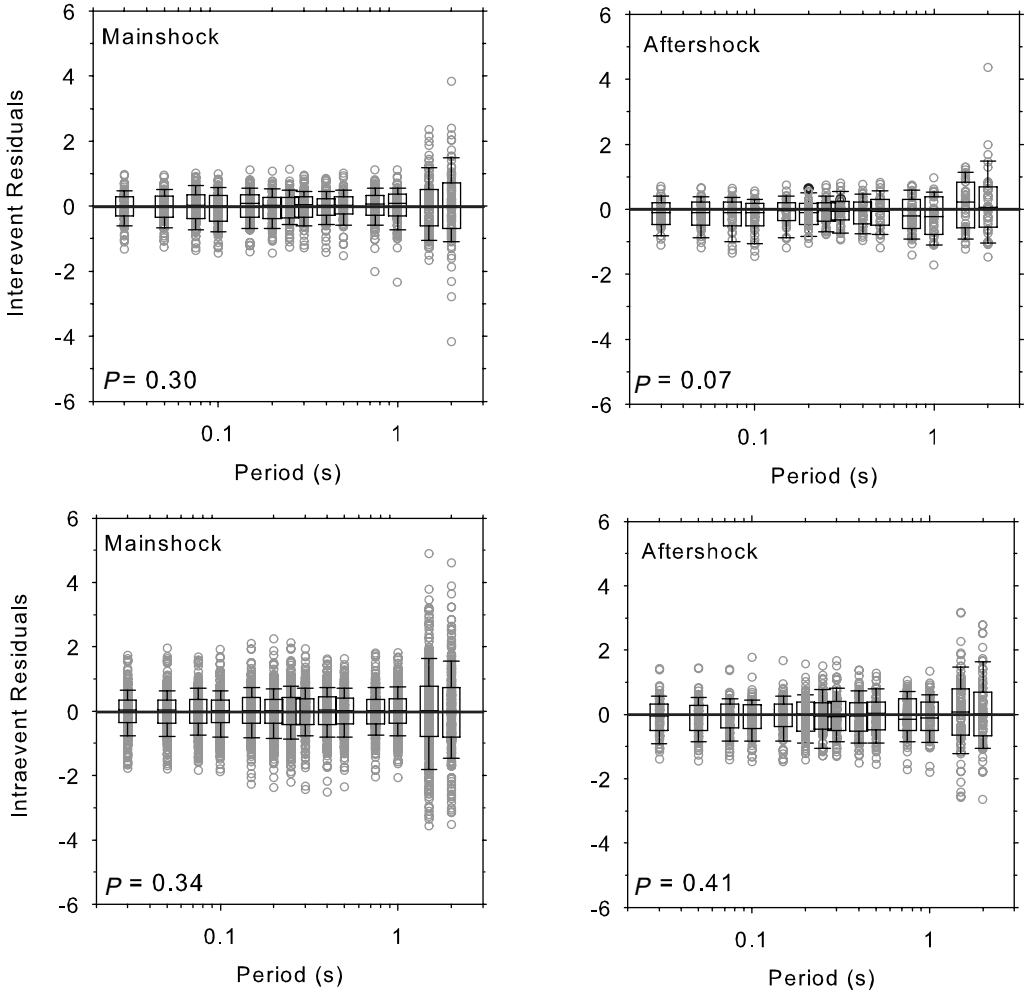

Figure 9. Period-dependent interevent (top row) and intraevent (bottom row) residual distributions for mainshock records (left panels) and aftershock records (right panels). The lower and upper edges of error boxes represent the first and third quartiles for each period-dependent residual bin, respectively. The horizontal lines in the middle section of error boxes show the median values, whereas the upper and lower caps of each error box correspond to the 16th and 84th percentile of residual distributions. Each panel presents the p value to measure the level of bias (existence of any remarkable trends in the residuals) in the mainshock and aftershock ground-motion estimations.

vibration period and have V_{S30} values greater than 450 m/s. This observation may partially explain the trends in Figure 7. Although not shown here due to space concerns, the period-dependent interevent residual variations of outlier events in our database draw more stable trends with vibration period, thus advocating the complex interaction between the local site conditions and ground motions. The simplicity of using chosen site response function is still appealing, and its improvement with the updated Turkish strong-motion database would certainly enhance our site-dependent estimations.

Figure 9 illustrates the period-dependent variation of interevent and intraevent residuals, with emphasis on the possible differences between the mainshock and aftershock ground-motion estimations. The residual plots in Figure 9 suggest that our GMPEs, in general, are unbiased both for mainshock and aftershock ground-motion estimations, although there is a slight tendency of overestimation for aftershocks. This bias can be neglected because the median values of period-dependent aftershock residual bins (horizontal lines in the middle part of each box plot) are almost zero. The large p values (presented in the lower left corner of each panel) also support this observation, advocating once again the lack of difference between mainshock and aftershock ground-motion estimations. Abrahamson *et al.* (2008) reported lower ground-motion estimations for GMPEs that include aftershock events, whereas Douglas and Halldórsson (2010) presented cases opposing this argument. Other studies (e.g., Boore and Atkinson, 1989; Atkinson, 1993) pointed to different scaling of ground-motion estimations upon the consideration of aftershocks without giving a description about the tendency of bias.

Comparisons with Local and Global Predictive Models

We compared our ground-motion estimations with the global GMPEs that are listed in Table 1. The NGA models consist of very large number of records for better magnitude and distance distributions to reduce the aleatory variability. Figure 10 shows the data distribution in the NGA models in terms of seismic regions (stacked bars). The immediate observation from this distribution is the dominance of California and Taiwan earthquakes in these models. Apparently, the NGA model developers considered negligibly a small number of data from Europe and the Middle East, as well as from the rest of the shallow crustal active seismic regions. The same figure also presents the country-based data distribution of the pan-European predictive model (pie chart). The data are primarily from three countries: Turkey, Greece, and Italy. In fact, recordings from Turkey and Italy cover almost 60% of the Akkar and Bommer (2010) GMPEs.

Figure 11 presents our comparisons for PGA_{GM}, PSA_{GM}, and PGV_{GM} at two magnitude levels: **M** 5 (representing small events) and **M** 7 (representing large events). These magnitudes correspond to the common lower and upper magnitude bounds of the considered models. Recent observations (e.g., Akkar and Bommer, 2010; hereafter referred to as AB10) recommend that comparisons between predictive models should not only depend on the median estimations but should also consider different percentiles to discover their overall characteristics. We adopted this approach and present our comparisons for median (middle panels) and median ±sigma (end panels) ground motions. We used a reference site class with $V_{S30} = 760$ m/s for the overall comparisons because of the lack of uniformity in site classification among the considered GMPEs. We did not make any fine-tuning between the horizontal component definitions GMRotI50 (NGA models) and GM (AB10 and this study) because, on average, they yield the same values for the ground-motion components of interest (Beyer and Bommer, 2006; Campbell and Bozorgnia, 2006). We assumed vertical (dip = 90°) strike-slip faulting in our comparisons. Some NGA models (i.e., Abrahamson and Silva, 2008 [AS08]; Campbell and Bozorgnia, 2008 [CB08], and Chiou and Youngs, 2008 [CY08]) consider the depth to top-of-rupture (Z_{TOR}) and soil/sediment depth as additional explanatory variables in their ground-motion estimations. We used median Z_{TOR} values in Abrahamson *et al.* (2008) and the recommended soil/sediment depth of each model developer while implementing these GMPEs in our comparisons. AS08 can explicitly consider the difference between mainshock and aftershock events in the ground-motion estimations. We treated their model for mainshock events, assuming that it is more critical for the comparisons discussed here. We normalized the ground-motion estimations of global models by the estimations of our predictive model in the comparisons. This way, we quantitatively measured the discrepancy between our model and the global GMPEs.

Several observations can be made from the comparative plots presented in Figure 11. First, regardless of percentile, our ground-motion estimations are lower with respect to the global equations. The differences are more pronounced for median and median–sigma estimations. The latter case is due to the adverse effects of large sigma in our model. The discrepancies are significant for small magnitudes and reduce considerably with increasing magnitude. Low-amplitude ground motions observed at large-magnitude events in the Turkish strong-motion database can be one of the reasons for our lower estimations at large magnitudes. Although

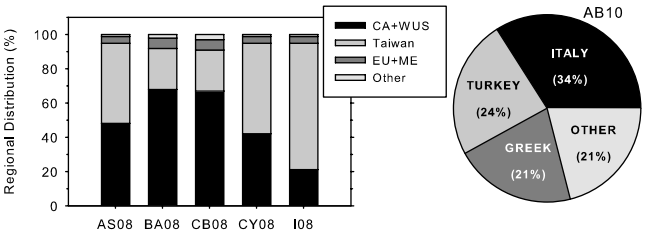

Figure 10. Regional distribution of the data in the NGA (left panel, stacked bars) and pan-European (right panel, pie chart) models. For NGA models: CA, California; WUS, western United States; EU + ME, Europe and the Middle East.

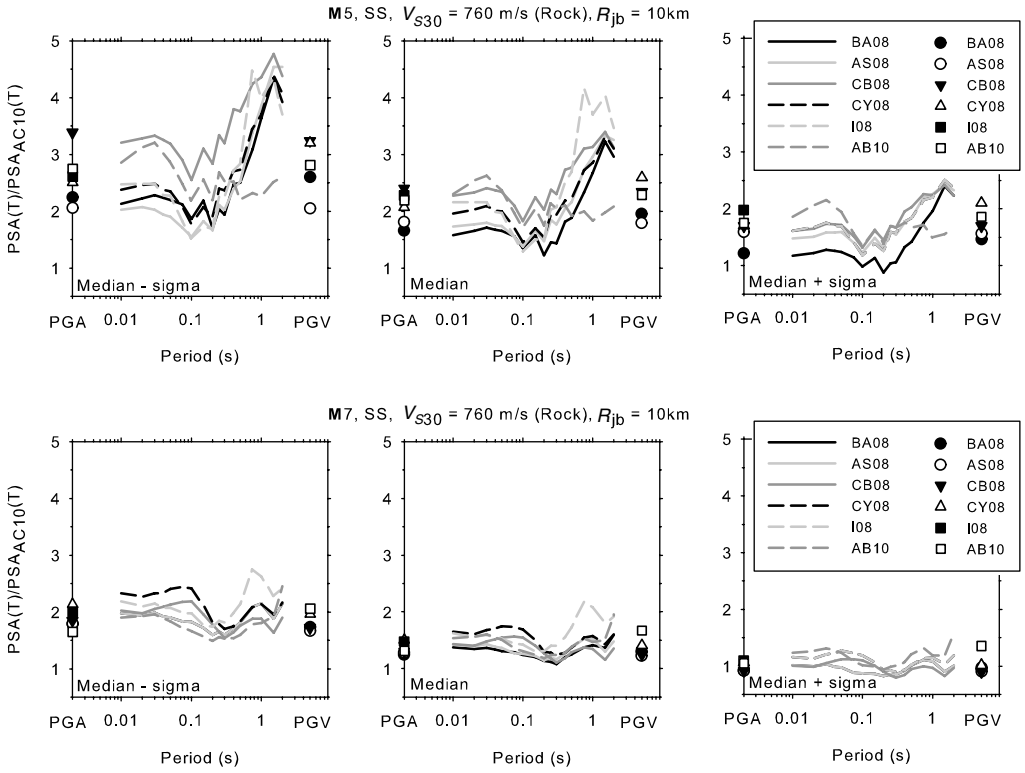

Figure 11. Normalized ground-motion estimations of the global GMPEs with respect to our prediction equations presented in this paper. The comparisons are for a small-magnitude (**M** 5) and a large-magnitude (**M** 7) strike-slip event at a rock site (V_{S30} = 760 m/s) that is 10 km (R_{jb}) from the seismic source. The dip angle of the strike-slip fault is 90°, and the magnitude-dependent depth to top-of-rupture parameter for some of the NGA models is taken from Abrahamson *et al.*, 2008.

our GMPEs do not show significant bias for aftershock estimations (see discussions about Fig. 9), their inclusion in our model may provoke the lower ground-motion estimations, particularly at small magnitudes. The strength of this remark, however, is debilitated because AB10, AS08, and CY08 also use the aftershock data in their predictive models (Note: We did not activate the aftershock flag in the Abrahamson and Silva, 2008, model so, strictly speaking, their estimations would reflect the mainshock features as in the case of BA08 and CB08.) The reduced differences between our model and the global models for larger magnitudes might be explained by the reliability of data for larger magnitude events. Another observation from these comparative plots is the large variation among the normalized curves (more emphasized in the small-magnitude case due to vertical axis scaling) advocating the existing discrepancies in the global GMPEs, a topic that has also been discussed in the recent articles by Douglas (2007), Abrahamson *et al.* (2008), and Bommer *et al.* (2010).

We further explored the differences between our model and the global GMPEs by deriving predictive equations for PGA_{GM} and PGV_{GM} using the combined Turkish and Italian strong-motion databases (hereinafter referred to as the ITRK database). We then compared our estimations with those of the recent pan-European model (Akkar and Bommer, 2010). Because PGA and PGV are assumed to represent high-frequency to intermediate-frequency ground-motion components, observations made from these comparisons can be valid for the spectral band considered in this paper. Figure 12 gives a general view about the magnitude and distance distributions of the ITRK and AB10 databases in terms of site classes. The databases draw fairly similar distributions for magnitude and distance. The ITRK dataset, with a total of 1004 recordings (almost twice that of the AB10 database), surmounts the deficient rock site and reverse fault events in the Turkish database that might be put forward as a weakness for our GMPEs. Considering the fact that AB10 is dominated significantly by the strong-motion recordings of Italy and Turkey, comparisons between AB10, our model, and the GMPEs obtained from the ITRK database would yield important information about the differences between regional and global models. (Note: Although AB10 consists of a considerable number of Turkish and Italian data, only one-third of Turkish and Italian records in AB10 overlap with the corresponding Turkish and Italian accelerograms in ITRK.)

We used the same regression technique (maximum likelihood) for the PGA_{GM} and PGV_{GM} GMPEs of the ITRK database. The functional form is the same one used in this paper except for the site effects. We classified the ITRK ground motions as rock, stiff, and soft soil site recordings with the V_{S30} intervals defined in AB10. Essentially, the GMPEs of the ITRK database use the linear site amplification model implemented in AB10. The comparative regression

results are presented in Figure 13. We used the same scenarios (i.e., **M** 5 and **M** 7 strike-slip events at rock sites) in these comparisons for a fair discussion with our previous observations presented in Figure 11. The plots in Figure 13 indicate that both PGA_{GM} and PGV_{GM} estimations of AB10 are larger than those obtained from the ITRK database and our model. The estimations become similar with increasing magnitude (i.e., with the **M** 7 scenario). These observations are similar to those made between our predictive equations and the global models considered in this study. Note that, except for small-magnitude events at short distances ($R_{jb} < 10$ km), our predictions almost overlap with those of the ITRK database. As stated previously, the ITRK database improves the ground-motion sampling with respect to the Turkish dataset for rock sites and reverse faults that apparently increase the stability of ground-motion estimations with a lesser influence on their magnitude and distance-dependent amplitudes.

Comparable observations between Figure 11 and Figure 13, as well as similar magnitude and distance distributions in the AB10 and ITRK databases, led us to investigate other seismological parameters that dominate ground-motion amplitudes. Departing from the influence of depth on the ground-motion amplitudes, we compared the depth distribution of the ITRK and AB10 databases in Figure 14. The distributions are based on the histograms with depth bins of 5-km intervals The plots also show the mean ($\mu_{\mathbf{M}}$) and standard deviation ($\sigma_{\mathbf{M}}$) of magnitudes in the bins that are approximately the same for both databases. The comparisons indicate deeper events in the ITRK database with respect to the depth distribution of AB10. Fairly similar mean magnitudes in the common depth bins of the ITRK and AB10 databases bring forward the significance of different depth variations in these databases that seem to play an important role on the ground-motion estimations. This observation is underscored further with the comparative depth distributions between the NGA GMPEs and our model (Fig. 15). These plots also suggest a relatively shallow depth composition of the NGA models with respect to the depth distribution

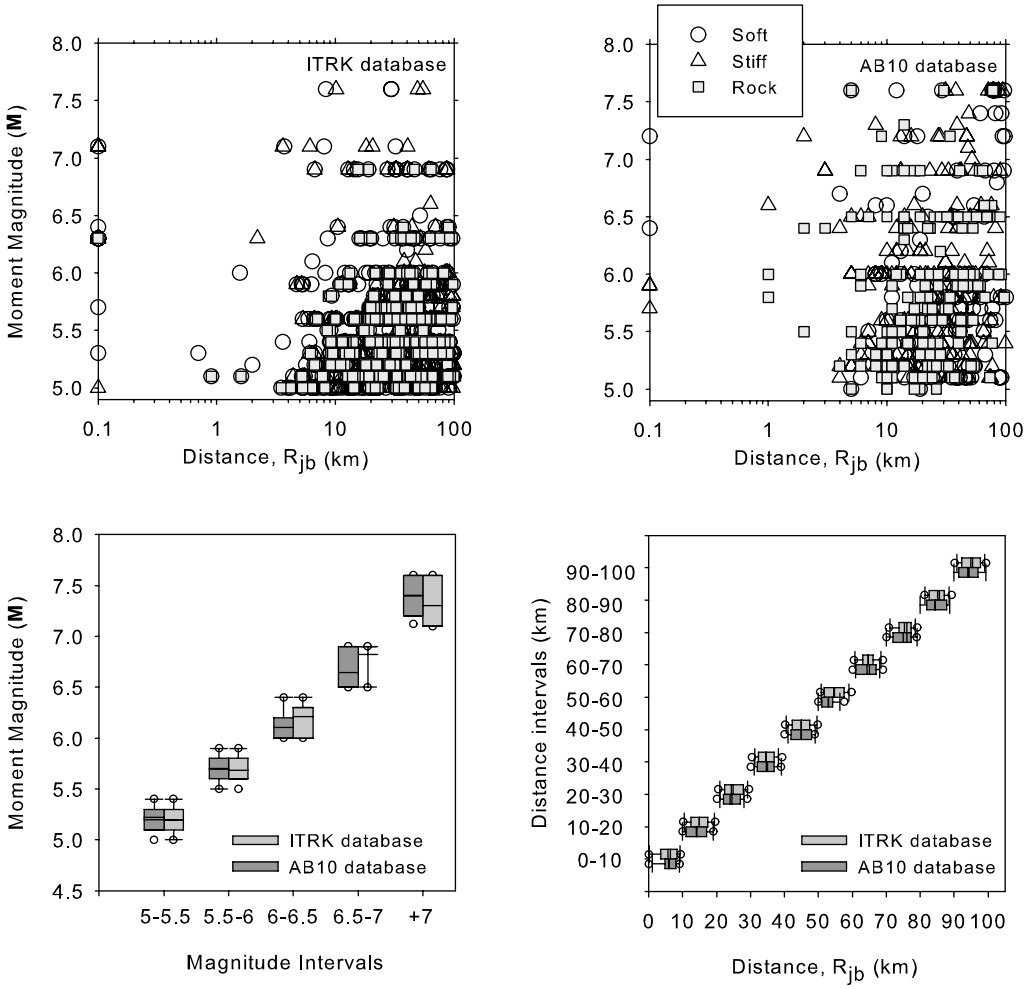

Figure 12. Comparisons of magnitude and distance distribution between the ITRK and AB10 databases. Top row: magnitude versus distance scatters for these two databases in terms of soft (180 m/s $\leq V_{S30} <$ 360 m/s), stiff (360 m/s $\leq V_{S30} <$ 760 m/s), and rock ($V_{S30} \geq$ 760 m/s) site conditions. Bottom row: compares the median (central horizontal bar in the box plots) and 16th and 84th percentile (lower and upper edges of the box plots) fractiles of moment (left panel) and distance (right panel) distributions of the same databases for predefined magnitude and distance intervals.

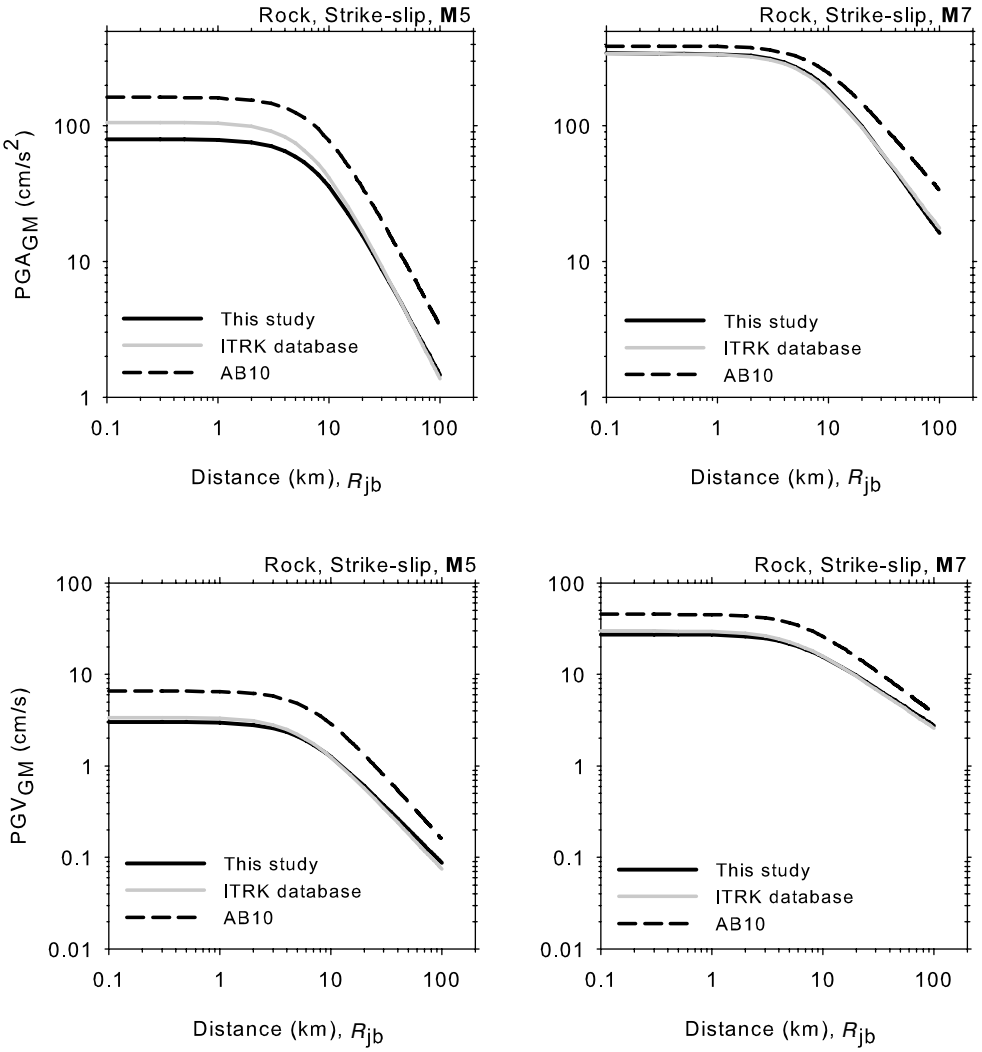

Figure 13. Comparisons of PGA_{GM} (top row) and PGV_{GM} (bottom row) estimations at rock sites from the predictive models of this study, AB10, and the ITRK database. The left and right columns compare small (**M** 5) and large (**M** 7) events for strike-slip faulting, respectively.

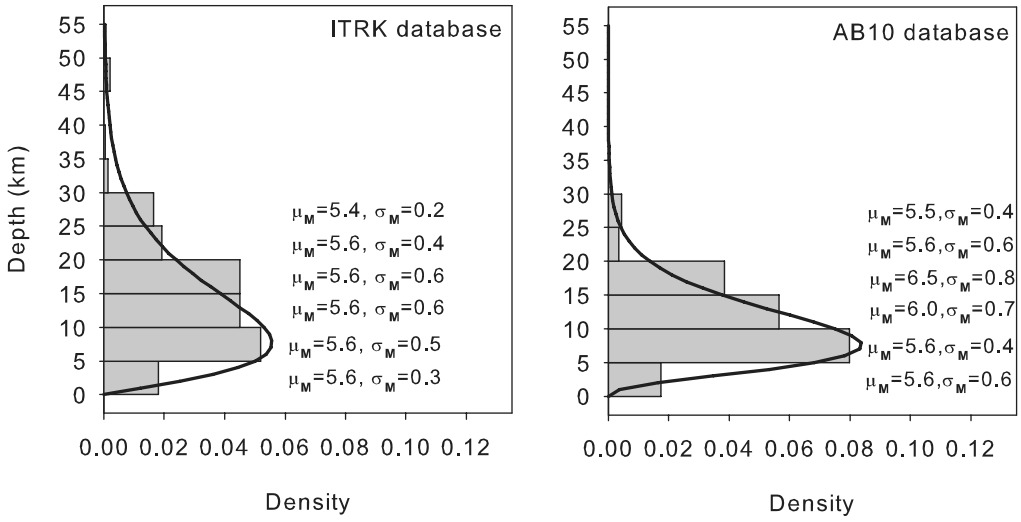

Figure 14. Depth distributions of the ITRK (left panel) and AB10 (right panel) databases. The histograms are plotted for a depth interval of 5 km. $\mu_{\mathbf{M}}$ and $\sigma_{\mathbf{M}}$ show the mean and standard deviation of magnitude in each depth bin, respectively.

in the Turkish database. The relatively complicated seismotectonic settings for Turkey, due to the complex deformations resulting from the continental collision between the African and Eurasion plates, describe a crustal thickness variation of 25–40 km from western to eastern Turkey (Tezel *et al.*, 2007). This information is consistent with the depth distribution of our database (Fig. 15) that seems to be a prominent factor in the lower Turkish ground motions.

Summary and Conclusions

In this study, we introduced a new set of regional GMPEs for Turkey for magnitude and distance ranges of $5.0 \leq \mathbf{M} \leq 7.6$ and $R_{jb} \leq 200$ km using the recently compiled Turkish strong-motion dataset. The new GMPEs estimate PGA_{GM}, PGV_{GM}, and 5%-damped PSA_{GM} between $0.03 \text{ s} \leq T \leq 2.0$ s through a functional form that accounts for style of faulting, nonlinear soil behavior, and magnitude-dependent saturation and decay effects. We then explored the differences between the local and global predictive models by comparing our new model with the NGA and pan-European (Akkar and Bommer, 2010) global GMPEs. As part of these comparisons we derived prediction equations on PGA_{GM} and PGV_{GM} using a combined Turkish and Italian ground-motion dataset to complement our observations for the differences between local and global GMPEs.

Our studies on the data distribution of global models show that their databases are confined to some specific regions and countries and reflect the shallow active seismicity based on the seismotectonic settings in those locations. Our ground-motion estimations are low with respect to the global models investigated here. The discrepancies are significant at small magnitudes and decrease toward larger magnitudes. In this study, we tried to explain this observation by emphasizing the significance of depth that is not fully considered in the investigated ground-motion models but that its variation can affect the ground-motion estimations, depending on the regional seismotectonic settings. In essence, our comparisons between the GMPEs of this study, Akkar and Bommer (2010), and the combined Italian and Turkish database (ITRK) suggest that depth distribution becomes important on the differences between local and global GMPEs. We come to this conclusion because the ITRK database has a denser data population and comparable magnitude-versus-distance resolution with respect to the Akkar and Bommer (2010) model but differs in depth distribution, in particular towards deeper events, which results in lower ground-motion estimations with respect to the Akkar and Bommer (2010)

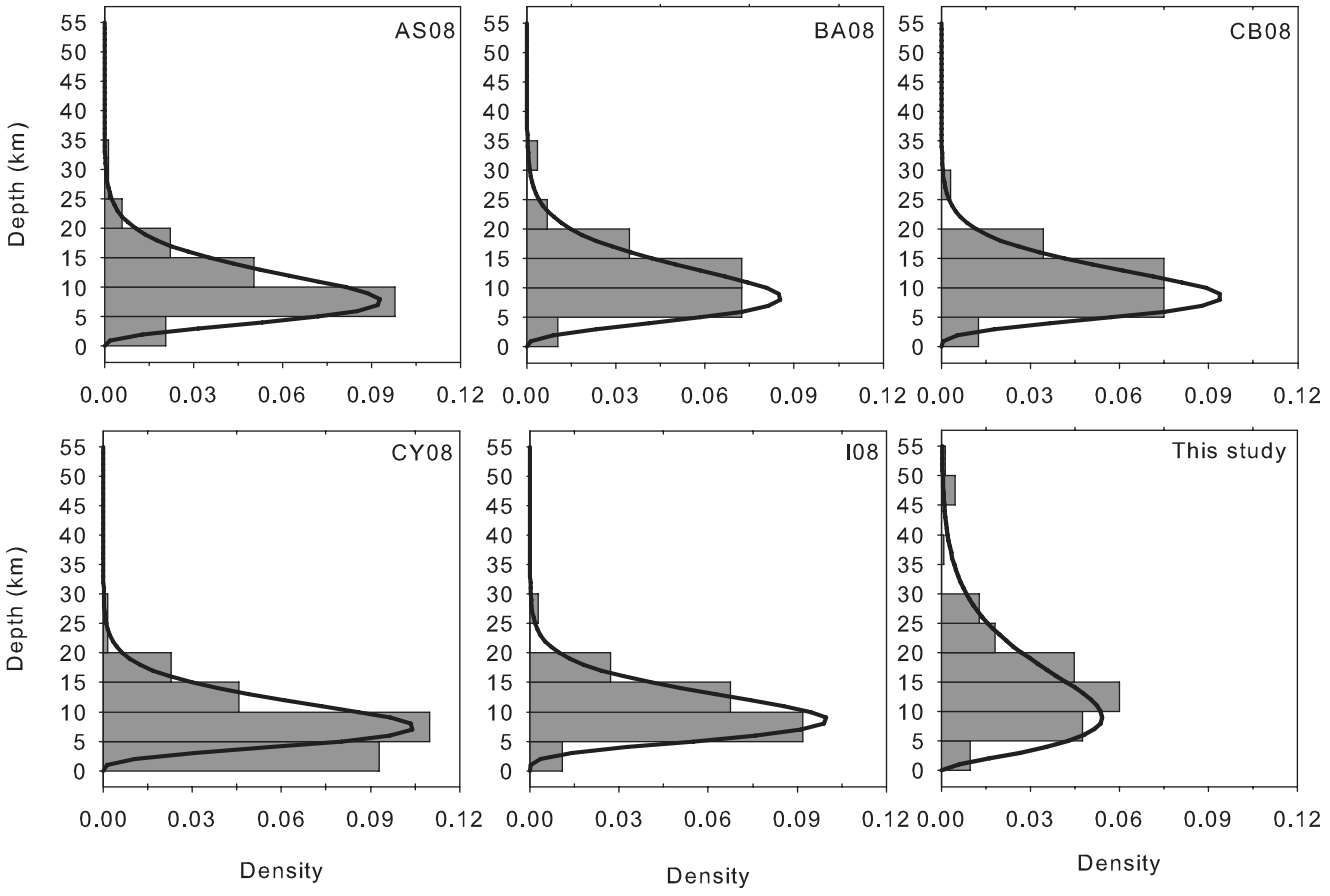

Figure 15. Comparative depth distributions between our predictive model (bottom right corner) and the NGA models.

GMPEs. This conclusion is augmented by the similar ground-motion estimations of the ITRK database and those of our GMPEs that are due to their comparable depth distributions. As a matter of fact, the differences between the depth distributions of NGA models and our model toward deeper events could be one of the strong reasons behind the discrepancies between the Turkish and NGA GMPEs that give more emphasis to the importance of the depth distribution that may stem from the seismotectonic settings of the regions of interest.

Data and Resources

The Turkish ground motions are obtained from the web site http://daphne.deprem.gov.tr:89/ operated and maintained by the Earthquake Division of the Turkish Disaster and Emergency Management Agency. The Italian accelerometric data are provided by the Milano Section of Istituto Nazionale di Geofisica e Vulcanologia and is available from http://itaca.mi.ingv.it/ItacaNet/.

The "Compilation of Turkish Strong-Motion Network According to the International Standards" project is conducted by the Earthquake Engineering Research Center of the Middle East Technical University and the Earthquake Division of the Turkish Disaster and Emergency Management Agency.

Acknowledgments

This study is financially supported by the project entitled "Compilation of Turkish Strong-Motion Network According to the International Standards," which is granted by the Scientific and Technological Council of Turkey under the award no. 105G016. Julian Bommer from Imperial College, David M. Boore from the U.S. Geological Survey at Menlo Park, California, and Kenneth W. Campbell from EQECAT Inc. made valuable suggestions during the preparation stage of this manuscript. Constructive critiques of Dino Bindi, two anonymous reviewers, and *BSSA* associate editor Gail Atkinson resulted in a significant improvement in the technical quality of the paper. We also thank Francesca Pacor, Lucia Luzi, and Marco Massa for providing the ITACA dataset. Margaret Segou helped us in the crustal depth variation of Turkey. Our graduate students, Emrah Yenier and Abdullah Sandıkkaya, processed many records and compiled the entire dataset. They helped us in many stages of this paper. We also extend our sincere gratitude to them.

References

Abrahamson, N. A., and W. J. Silva (1997). Empirical response spectral attenuation relations for shallow crustal earthquakes, *Seismol. Res. Lett.* **68,** 94–127.

Abrahamson, N. A., and W. Silva (2008). Summary of the Abrahamson and Silva NGA ground motion relations, *Earthq. Spectra* **24,** 67–98.

Abrahamson, N. A., G. Atkinson, D. M. Boore, Y. Bozorgnia, K. Campbell, B. Chiou, I. M. Idriss, W. Silva, and R. Youngs (2008). Comparison of the NGA ground-motion relations, *Earthq. Spectra* **24,** 45–66.

Akkar, S., and J. J. Bommer (2006). Influence of long-period filter cut-off on elastic spectral displacements, *Earthq. Eng. Struct. Dynam.* **35,** 1145–1165.

Akkar, S., and J. J. Bommer (2007a). Empirical prediction equations for peak ground velocity derived from strong-motion records from Europe and the Middle East, *Bull. Seismol. Soc. Am.* **97,** 1275–1301.

Akkar, S., and J. J. Bommer (2007b). Prediction of elastic displacement response spectra in Europe and the Middle East, *Earthq. Eng. Struct. Dynam.* **36,** 1275–1301.

Akkar, S., and J. J. Bommer (2010). Empirical equations for the prediction of PGA, PGV and spectral accelerations in Europe, the Mediterranean region and the Middle East, *Seismol. Res. Lett.* **81,** 195–206.

Akkar, S., Z. Çagnan, E. Yenier, Ö. Erdoğan, A. Sandıkkaya, and P. Gülkan 2010). The recently compiled Turkish strong motion database: Preliminary investigation for seismological parameters, *J. Seismol.* **14,** 457–479.

Ambraseys, N. N., J. Douglas, S. K. Sarma, and P. M. Smit (2005). Equations for the estimation of strong ground motions from shallow crustal earthquakes using data from Europe and the Middle East: horizontal peak ground acceleration and spectral acceleration, *Bull. Earthq. Eng.* **3,** 1–53.

Atkinson, G. M. (1993). Earthquake source spectra in eastern North America, *Bull. Seismol. Soc. Am.* **83,** 1778–1798.

Atkinson, G. M., and M. Morrison (2009). Regional variability in ground motion amplitudes along the west coast of North America, *Bull. Seismol. Soc. Am.* **99,** 2393–2409.

Beyer, K., and J. J. Bommer (2006). Relationships between median values and between aleatory variabilities for different definitions of the horizontal component of motion, *Bull. Seismol. Soc. Am.* **96,** 1512–1522.

Bindi, D., L. Luzi, M. Massa, and F. Pacor (2010). Horizontal and vertical ground motion prediction equations derived from the Italian Accelerometric Archieve (ITACA), *Bull. Earthq. Eng.* **8,** no. 5, 1209–1230, doi 10.1007/s10518-009-9130-9.

Bommer, J. J., P. Stafford, and S. Akkar (2010). Current empirical ground-motion prediction equations for Europe and their application to Eurocode 8, *Bull. Earthq. Eng.* **8,** 5–26.

Bommer, J. J., P. Stafford, J. Alarcon, and S. Akkar (2007). The influence of magnitude range on empirical ground-motion prediction, *Bull. Seismol. Soc. Am.* **97,** 2152–2170.

Boore, D. M., and G. Atkinson (1989). Spectral scaling of the 1985 to 1988 Nahanni, Northwest Territories, earthquakes, *Bull. Seismol. Soc. Am.* **79,** 1736–1761.

Boore, D. M., and G. M. Atkinson (2008). Ground-motion prediction equations for the average horizontal component of PGA, PGV, and 5%-damped PSA at spectral periods between 0.01 s and 10.0 s, *Earthq. Spectra* **24,** 99–138.

Boore, D. M., J. Watson-Lamprey, and N. A. Abrahamson (2006). GMRotD and GMRotl: Orientation independent measures of ground motion, *Bull. Seismol. Soc. Am.* **96,** 1502–1511.

Building Seismic Safety Council (BSSC) (2009). NEHRP Recommended Seismic Provisions for New Buildings and Other Structures, *Report No. FEMA P-750*, National Institute of Building Sciences, Washington, D.C., available at http://www.nibs.org/index.php/bssc/publications/2009/ (last accessed September 2010).

Campbell, K. W. (1997). Empirical near-source attenuation relationships for horizontal and vertical components of peak ground acceleration, peak ground velocity, and pseudo-absolute acceleration response spectra, *Seismol. Res. Lett.* **68,** 154–179.

Campbell, K. W., and Y. Bozorgnia (2006). Next Generation Attenuation (NGA) empirical ground motion models: Can they be used in Europe?, *Proc. of the 1st European Conf. on Earthquake Engineering and Seismology*, paper no. 458Geneva, Switzerland, 3–8 September 2006.

Campbell, K. W., and Y. Bozorgnia (2008). NGA ground motion model for the geometric mean horizontal component of PGA, PGV, PGD and 5% damped linear elastic response spectra for periods ranging from 0.01 to 10 s, *Earthq. Spectra* **24,** 139–171.

Chiou, B. S.-J., and R. Youngs (2008). An NGA model for the average horizontal component of peak ground motion and response spectra, *Earthq. Spectra* **24,** 173–215.

Choi, Y., and J. P. Stewart (2005). Nonlinear site amplification as function of 30 m shear wave velocity, *Earthq. Spectra* **21,** 1–30.

Cotton, F., G. Pousse, and F. Bonilla (2008). On the discrepancy of recent European ground motion observations and predictions from empirical

models: Analysis of KiK-net accelerometric data and point-source stochastic simulation, *Bull. Seismol. Soc. Am.* **98,** 2244–2261.

Douglas, J. (2007). On the regional dependence of earthquake response spectra, *ISET J. Earthq. Technol.* **44,** 71–99.

Douglas, J., and D. M. Boore (2010). High-frequency filtering of strong-motion records, *Bull. Earthq. Eng.*, doi 10.1007/s10518-010-9208-4.

Douglas, J., and B. Halldórsson (2010). On the use of aftershocks when deriving ground-motion prediction equations, *Proc. in 9th U.S. National and 10th Canadian Conf. on Earthquake Engineering*, Toronto, Canada, 5–29 July 2010.

Douglas, J., and P. M. Smit (2001). How accurate can strong ground motion attenuation relations be?, *Bull. Seismol. Soc. Am.* **91,** 1917–1923.

Drouet, S., F. Scherbaum, F. Cotton, and A. Souriau (2007). Selection and ranking of ground motion models for seismic hazard analysis in the Pyrenees, *J. Seismol.* **11,** 87–100.

Erdoğan, Ö. (2008). Main seismological features of recently compiled Turkish strong-motion database, *M.Sc. Thesis*, Department of Civil Engineering, Middle East Technical University, Ankara, Turkey.

Hintersberger, E., F. Scherbaum, and S. Hainzl (2007). Update of likelihood-based ground-motion model selection for seismic hazard analysis in western central Europe, *Bull. Earthq. Eng.* **5,** 1–16.

Idriss, I. M. (2008). An NGA empirical model for estimating the horizontal spectral values generated by shallow crustal earthquakes, *Earthq. Spectra* **24,** 217–242.

Joyner, W. B., and D. M. Boore (1993). Methods for regression analysis of strong-motion data, *Bull. Seismol. Soc. Am.* **83,** 469–487.

Kagawa, T., K. Irikua, and P. G. Somerville (2004). Differences in ground motion and fault rupture between the surface and buried rupture earthquakes, *Earth Planets Space* **56,** 3–14.

Kalkan, E., and P. Gülkan (2004). Site-dependent spectra derived from ground motion records in Turkey, *Earthq. Spectra* **20,** 1111–1138.

Luzi, L., S. Hailemikael, D. Bindi, F. Pacor, and F. Mele (2008). ITACA (Italian accelerometric archive): A web portal for the dissemination of Italian strong motion data, *Seismol. Res. Lett.* **79,** 716–722.

Özbey, C., A. Sarı, L. Manuel, M. Erdik, and Y. Fahjan (2004). An empirical attenuation relationship for northerwestern Turkey ground motion using a random effects approach, *Soil Dynam. Earthq. Eng.* **24,** 115–125.

Power, M., B. Chiou, N. Abrahamson, Y. Bozorgnia, T. Shantz, and C. Roblee (2008). An overview of the NGA project, *Earthq. Spectra* **24,** 3–21.

Sandıkkaya, M. A., M. T. Yılmaz, B. B. Bakır, and Ö. Yılmaz. (2010). Site classification of Turkish national strong-motion stations, *J. Seismol.* **14,** 543–563.

Stafford, P. J., F. O. Strasser, and J. J. Bommer (2008). An evaluation of the applicability of the NGA models to ground motion prediction in the Euro-Mediterranean region, *Bull. Earthq. Eng.* **6,** 149–177.

Strasser, F. O., N. A. Abrahamson, and J. J. Bommer (2009). Sigma: Issues, insights, and challenges, *Seismol. Res. Lett.* **80,** 40–56.

Tezel, T., M. Erduran, and Ö Alptekin (2007). Crustal shear wave velocity structure of Turkey by surface wave dispersion analyisis, *Ann. Geophys.* **50,** 177–190.

Ulusay, R., E. Tuncay, H. Sönmez, and C. Gökçeoğlu (2004). An attenuation relationship based on Turkish strong motion data and iso-acceleration map of Turkey, *Eng. Geol.* **74,** 265–291.

Youngs, R. R., N. A. Abrahamson, F. I. Makdisi, and K. Sadigh (1995). Magnitude-dependent variance of peak ground acceleration, *Bull. Seismol. Soc. Am.* **85,** 1161–1176.

Earthquake Engineering Research Center
Department of Civil Engineering
Middle East Technical University (Main Campus)
06531 Ankara, Turkey
sakkar@metu.edu.tr
(S.A.)

Department of Civil Engineering
Middle East Technical University (Northern Cyprus Campus)
Kalkanlı Güzelyurt, KKTC
Mersin 10, Turkey
cagnan@metu.edu.tr
(Z.Ç.)

Manuscript received 27 November 2009